Modified hydraulic conductivity equations of bentonite-based materials under saturated and unsaturated conditions

Authors: Lin-yong Cui, Chao Zhou* and Wei-min Ye

*Corresponding author

Information of the authors:

First author: Dr Lin-yong Cui

Postdoctoral fellow, Department of Civil and Environmental Engineering, The Hong Kong Polytechnic University, Hung Hom, Hong Kong. E-mail: linyong.cui@polyu.edu.hk

Corresponding author: Dr Chao Zhou

Associate Professor, Department of Civil and Environmental Engineering, The Hong Kong Polytechnic University, Hung Hom, Hong Kong; Hong Kong Polytechnic University Shenzhen Research Institute, Shenzhen, China. E-mail: c.zhou@polyu.edu.hk

Co-author: Dr Wei-min Ye

Professor, Department of Geotechnical Engineering, College of Civil Engineering, Tongji University, Shanghai, China. E-mail: ye_tju@tongji.edu.cn

Abstract

Determining the hydraulic conductivity of bentonite-based materials holds paramount importance in the design of deep geological repositories for the radioactive waste disposal. Due to the substantial presence of strongly adsorbed water in bentonite-based materials, existing models often fail to accurately calculate their hydraulic conductivities. This study first proposed a method to quantify the volume of both capillary and adsorptive water within bentonite-based materials based on the crystallographic information of montmorillonite mineral. Then, calculating the hydraulic conductivities for both saturated and unsaturated bentonite-based materials are improved by considering the different roles of capillary and adsorptive water. At saturated conditions, capillary water dominates the water flow, and the Kozeny-Carman equation was modified to calculate the saturated hydraulic conductivity by subtracting the surface area and void ratio of adsorptive water pores. For unsaturated conditions, a new water retention model was developed. It is represented by a piecewise and continuous function that distinguishes between capillarity-dominated and adsorption-dominated processes. This water retention model is analytically integrable to be used with the Mualem model for calculating the relative hydraulic conductivity. Verifications show that the proposed equations can successfully determine the hydraulic conductivities of bentonite-based materials under saturated and unsaturated conditions.

Keywords: radioactive waste disposal; bentonite-based materials; hydraulic conductivity; soil-water retention curve; suction.

1. Introduction

Deep geological repository at depths ranging from 500 to 1000 meters emerges as the most viable approach for many countries for disposal of high-level radioactive waste (Cui et al., 2022, 2023). Bentonite-based materials (e.g., compacted bentonite, mixtures of bentonite with sand) are widely acknowledged as a good candidate for buffer/backfill materials in deep geological repositories (Wang et al., 2013; Cui et al., 2019; Xiang et al., 2020). For example, in the French repository concept, bentonite/sand mixtures are compacted and assembled to create an integrated buffer structure. This structure is designed to seal disposal pits through the gradual swelling of bentonite after underground water infiltration (Liu et al., 2015). Bentonite provides excellent swelling properties and low permeability when fully or nearly fully water-saturated, while sand is incorporated to enhance the thermal conductivity and mechanical stability of the non-saturated region (Liu et al., 2014). Following the recommendation of the International Atomic Energy Agency (IAEA), the saturated hydraulic conductivity of the buffer and backfill materials should fall below 10^{-13} m/s. Experimental measurement of such a low hydraulic conductivity is usually time-consuming, so models for calculating the saturated/ unsaturated hydraulic conductivity of bentonite are highly desired.

To determine the hydraulic conductivity, it is essential to understand the microstructure and water configuration within bentonite-based materials. Fig. 1 illustrates the microstructure of bentonite and the types of pore water within it (Bradbury and Baeyens, 2003; Tournassat et al., 2015). Compacted bentonite exhibits two distinct types of pores: smaller pores containing interlayer water and larger pores situated between the soil particles. Water in interlayer pores is strongly adsorbed onto the internal basal surfaces of montmorillonite layers or bonded on the exchangeable cations between interlayer space (Lu, 2016), exhibiting relatively low mobility. In contrast, larger pores between the montmorillonite and non-montmorillonite particles contain both free water and water influenced by diffuse double layer (DDL) (Bourg et al., 2003, 2006; Bradbury and Baeyens, 2003; Wersin et al., 2004), as illustrated in Fig. 1(c). Water in larger pores exhibits significantly higher mobility compared to interlayer water. Although DDL-influenced water in larger pores can be partially constrained due to interactions with charged external surfaces of the montmorillonite mineral, it still demonstrates greater mobility than interlayer pore water (Pusch and Yong, 2006). Based on these characteristics, "slow-moving" water in interlayer pores can be classified as adsorbed water, while "fast-moving" water in larger pores can be assigned as capillary water.

On the one hand, hydraulic radius theories, capillary models, statistical models, and empirical equations are commonly used for calculating the K_s of bentonite-based materials, (Alyamani and Şen, 1993; Koltermann and Gorelick, 1995; Chapuis, 2002; Chapuis and Aubertin, 2003). Among these, the Kozeny-Carman (KC) equation, originally proposed by Kozeny (1927) and later modified by Carman (1937), is frequently cited, and widely utilized for calculating K_s. This equation assumes that the porous material consists of an assembly of capillary tubes and expresses K_s as a function of void ratio, specific surface area, and a factor that accounts for the shape and tortuosity of flow channels (Ng et al., 2024a, 2024b). Although the KC equation has been experimentally validated for coarse-grained soils such as sandy soils, its applicability to compacted clays is questionable (Carrier, 2003; Chapuis, 2012; Chen et al., 2021; Ruan et al., 2022), particularly in clays that exhibit secondary porosity (Chapuis and Aubertin, 2003). For bentonite-based materials, calculating K_s becomes more complex due to the distinct properties of interlayer water, DDL water and free water. Empirical relationships between hydraulic conductivity and basic soil parameters such as dry density and montmorillonite content are often used to determine K_s of bentonite (Dixon et al., 1999; Lloret and Villar, 2007; Komine, 2008). Recently, attempts have been made to modify the KC equation to determine K_s of bentonite-based materials. Since interlayer water exhibits relatively low mobility and has a limited impact on the water flow (Suzuki et al., 2005), Chen et al. (2021) and Ruan et al. (2022) have excluded the contributions of interlayer pores in their modifications of the KC equation. Note that, the interlayer pore volume and surface area can also be quantitatively determined from the crystallographic information of montmorillonite (Bourg et al., 2006; Tournassat and Appelo, 2011; Tournassat et al., 2015). This approach could provide a new perspective for modifying the KC equation, but the description performance of the modified KC model based on crystallographic information remains unknown and requires further investigation.

On the other hand, Yoon et al. (2021), Chen et al. (2021), and Ruan et al. (2022) employed empirical models that expressed the relative hydraulic conductivity K_r of bentonite-based materials, as a power function of effective water saturation, assuming constant power coefficient values of 3 (Ruan et al., 2022), 3.5 (Chen et al. 2021) or 1.01~3.35 (Yoon et al., 2021). However, these values lack sufficient physical significance. Statistical models address this limitation by incorporating factors such as pore size distribution, tortuosity and pore connectivity, in conjunction with the water soil-water retention curve (SWRC), to calculate the K_r. Incorporating the analytical expression of the SWRC into conductivity models, such as that of Burdine's or Mualem's models, yields the analytical solution for K_r (Ng et al., 2015a, 2015b). For unsaturated bentonite-based materials, both capillary water (existing in larger pores) and adsorbed water (within interlayer pores) could exist, and adsorptive force could dominate the water transport under high suction conditions (Romero et al., 2011). The conventional van Genuchten (1980) model is the most widely used SWRC model across the full suction range. While it performs well at medium to high water contents, it often yields poor descriptions at low water contents or high matric suctions (Rossi and Nimmo, 1994; Fayer and Simmons, 1995). Lu (2016) further noted that this model is derived empirically from the shape of the SWRC rather than being grounded in the underlying water retention mechanisms. Several SWRC equations capable of representing water retention at all suctions, while accounting for both adsorption and capillarity processes, have been formulated by previous researchers (e.g., Lu, 2016; Lebeau and Konrad, 2010; Revil and Lu, 2013). These models provide parameters with physical interpretations, resulting in satisfactory descriptions of water retention data. However, they generally involve more than five parameters, and the adsorbed water saturation is often treated as a fitting parameter. For bentonite-based materials, the water configuration within different pore types, interlayer pores and larger pores, can be quantitatively determined based on the crystallographic information of montmorillonite. This approach can also support the development of the SWRC models and the subsequent determination of unsaturated conductivity for bentonite-based materials.

This study begins by providing a method to quantify the capillary and adsorptive water volume within the bentonite-based materials based on the crystallographic information of montmorillonite. Following this, the K_s is derived through modifications to the conventional form of the KC equation, focusing solely on the contributions of capillary water to water flow. Unsaturated hydraulic conductivity is determined using a piecewise water retention function. This function delineates clear distinctions between capillarity-dominated and adsorption-dominated processes but ensures a continuous and smooth transition. These equations introduce a novel perspective for comprehending the hydraulic properties of partially and fully saturated bentonite-based materials.

2. Theoretical background

According to Lukasiewicz and Reed (1988), for the porous medium featuring a bundle of parallel but tortuous, non-interconnected channels of equal length L_e, Poiseuille's equation can be given as:

$$v = \frac{R_h^2}{k\mu} \cdot \frac{\Delta p}{L_e} \tag{1}$$

where k is a shape factor, μ represents the viscosity (Pa·s), and R_h denotes the hydraulic radius (m). Carman (1937) stated that relating the actual velocity in the pores v to the apparent velocity V through a porous medium, Dupuit's assumption should be modified by multiplying the ratio of actual channel length L_e to the specimen length L. Poiseuille's equation then becomes:

$$V = \left(\frac{\phi {R_h}^2}{\mu} \cdot \frac{\Delta p}{L}\right) \cdot \left(\frac{L^2}{k{L_e}^2}\right) \tag{2}$$

where ϕ is the overall porosity of the porous medium. kL_e^2/L^2, known as the Kozeny constant

$C_{K\text{-}C}$, is about 5.0 (Carman, 1937), which accounts for pore shape and tortuosity. The K_s for the porous medium can be given by:

$$K_s = (\frac{1}{C_{K-C}})(\frac{\gamma}{\mu}) \cdot \phi {R_h}^2 \tag{3}$$

where γ represents the unit weight (N/m^3). Assuming a uniform cross-section of the flow channel extends the definition of R_h as the ratio of the volume of fluid in pore channels to the channel surface area:

$$R_h = \frac{\text{Fluid volume in channel}}{\text{Channel surface area}} = \frac{e}{\rho_s SSA_s} \tag{4}$$

where e is the overall void ratio, ρ_s and SSA_s represent the density and specific surface area of soil particles, respectively. By substituting the expression for R_h from Eq. (4) into the K_s function in Eq. (3) yields the original form of the KC equation:

$$K_s = (\frac{1}{C_{K-C}})(\frac{\gamma}{\mu})(\frac{1}{\rho_s SSA_s})^2 \frac{e^3}{1+e} \tag{5}$$

The conventional KC equation models porous materials as an assembly of capillary tubes, representing the K_s as a function of void ratio, the specific surface area, shape factor and tortuosity of flow channels. However, the porosity in KC model is an effective-transport void ratio, which accounts for the cross-sectional area available for water flow when flow occurs solely in the pore space, while specific surface area was actually utilized to determine the surface area of these effective-transport void space. These two parameters can be smaller than the overall void ratio of the specimen and the total surface area of the soil particles, respectively, in cases where the porous media contains strongly adsorbed water, which has limited mobility. Therefore, for bentonite-based materials, it is necessary to adjust the model parameters based on the water type when applying the KC model to calculate the hydraulic conductivity.

3. Saturated hydraulic conductivity of bentonite-based materials

In this study, the basic concept for modifying the KC equation is to establish a dual-pore system filled with capillary and adsorbed water, respectively. Within this system, the contribution of adsorbed water (interlayer water) to flow is neglected since it has limited mobility as compared to capillary water (DDL water and free water) under saturated conditions (Bourg et al., 2003; Pusch and Yong, 2006). Therefore, it is assumed that water flow exclusively takes place in the capillary water-filled pores, which can be further described by modifying the conventional KC equation.

3.1 Modifications to the Kozeny-Carman equation

For bentonite-based materials, modifications to parameters of porosity ϕ and hydraulic radius R_h are conducted by considering only contributions of capillary water. In this regard, R_h can be modified as:

$$R_h = \frac{e_{ca}}{\rho_s SSA_{ca}} \tag{6}$$

where e_{ca} represents the void ratio of pores containing capillary water, and SSA_{ca} represents the reduced specific surface area, corresponding to the contact area with only capillary water. Meanwhile, replacing the overall porosity ϕ in Eq. (3) with the porosity of capillary water pores $\phi_{ca} = e_{ca}/(1+e)$ and applying the modified expression of R_h (Eq. (6)) to the K_s function in Eq. (3) yields the modified KC equation for bentonites:

$$K_s = (\frac{1}{C_{K-C}})(\frac{\gamma}{\mu})(\frac{1}{\rho_s^2 SSA_{ca}^2})(\frac{e_{ca}{}^3}{1+e}) \tag{7}$$

where γ and μ represent unit weight and the viscosity of capillary water. In Eq. (7), if all the water within a porous medium resides in the pore space is capillary water, actively participating in water flow, then $e_{ca} = e$, and $SSA_{ca} = SSA_s$, and Eq. (7) reverts to the conventional KC equation. For bentonite materials, the prerequisite for Eq. (7) to calculate the K_s is to ascertain the capillary water void ratio e_{ca} and reduced specific surface area SSA_{ca}. They are described in the next section.

3.1 Capillary water void ratio for bentonite-based materials

Fig. 2 presents the composition of the bentonite-sand mixtures for bentonite-based materials (bentonites or bentonite-sand mixtures). The basic volume-mass relationships can be expressed as:

$$\rho_d = \frac{m_s}{V_s + V_v} \tag{8}$$

$$m_s = m_m + m_{nm} + m_{sand} \tag{9}$$

$$V_s = V_m + V_{nm} + V_{sand} \tag{10}$$

$$\omega_1 = \frac{m_m}{m_m + m_{nm}} = \frac{\rho_m V_m}{\rho_m V_m + \rho_{nm} V_{nm}} \tag{11}$$

$$\alpha = \frac{m_m + m_{nm}}{m_m + m_{nm} + m_{sand}} = \frac{\rho_m V_m + \rho_{nm} V_{nm}}{\rho_m V_m + \rho_{nm} V_{nm} + \rho_{sand} V_{sand}} \tag{12}$$

where ρ_d is the dry density of specimen, V_s is the total volume of solid particles in the mixture, V_v is the volume of the void space in the mixture, and m_s is the dry mass of sand and bentonite in the mixture. ρ_m, ρ_{nm} and ρ_{sand} denote the density of montmorillonite mineral in bentonite, minerals excluding montmorillonite in bentonite and sand, respectively. V_m, V_{nm} and V_{sand} are the volume of montmorillonite mineral in bentonite, minerals excluding montmorillonite in bentonite and sand, respectively. m_m, m_{nm} and m_{sand} are the dry mass of montmorillonite in the bentonite, minerals excluding montmorillonite in bentonite, and sand in bentonite-sand mixtures, respectively. ω_1 is the mass content of montmorillonite in bentonite, and α is the content of bentonite in bentonite-sand mixtures by mass, with $\alpha = 1$ for pure bentonite materials. Specifically, for bentonite-based materials, the density of the soil particle ($\rho_s = m_s/V_s$), can be determined by combining Eqs. (9)~(12):

$$\rho_s = \frac{\rho_m \cdot \frac{1}{\alpha} \cdot \frac{1}{\omega_1}}{1 + (\frac{1}{\omega_1} - 1) \cdot \frac{\rho_m}{\rho_{nm}} + (\frac{1}{\alpha} - 1) \cdot \frac{1}{\omega_1} \frac{\rho_m}{\rho_{sand}}} \tag{13}$$

As depicted in Fig. 1(a), the fundamental structure of montmorillonite mineral, which is the predominant clay mineral within bentonite, is comprised of one octahedral sheet (edge-sharing $M_{Oct}O_6$ octahedra, M_{Oct}=Al, Mg or Fe) and two tetrahedral sheets (corner-sharing $M_{Tet}O_4$ tetrahedra, M_{Tet}=Si or Al). These three sheets combine to form a montmorillonite layer (TOT layer) with a thickness of 9.6 Å (Appelo, 2013). Typically, these TOT layers are stacked together to form montmorillonite particles (Fig. 1(b)).

As shown in Fig. 1(b), the adsorbed water (interlayer water) volume in bentonite materials can be determined from the internal basal surface area and the interlayer distance of montmorillonite (Kozaki et al., 2001; Bourg et al., 2006). For bentonite-based materials, the adsorbed water volume can be given by:

$$V_{in} = \frac{A_{in} h_{in}}{2} \cdot m_s \omega \tag{14}$$

where V_{in} represents the adsorbed water volume (m^3), A_{in} and h_{in} are the internal basal surface area per unit mass of montmorillonite (m^2/g) and interlayer distance (m), respectively, m_s is the dry mass of bentonite (g) and ω represents the content of montmorillonite in bentonite-based materials by mass. Note that, for bentonite-sand mixtures, $\omega = \omega_1\alpha$, while for bentonite materials, $\omega = \omega_1$ (with $\alpha = 1$).

The internal basal surface area A_{in} in Eq. (14) can be determined based on the crystallographic information of montmorillonite. As shown in Fig. 1(a), the structure of the montmorillonite unit cell exhibits a monoclinic unit cell with dimensions of $a \times b \times c^* = 0.523 \times 0.905 \times 0.96$ nm^3 (Appelo, 2013). Here, c^* represents the orthogonally projected c-axis of the monoclinic unit cell, and is equal to the sum of the interlayer distance and layer thickness (Madsen, 1998), i.e., $c^* \approx h_{in} + 0.96$ (nm). The unit cells are stacked for a montmorillonite particle, with the stacking number of n_a, n_b, and n_c along the a, b and c dimensions, respectively. Based on the crystallographic information, Appelo (2013) proposed the following equation to calculate the internal basal surface area per unit mass A_{in}:

$$A_{in} = \frac{2n_a a \cdot n_b b \cdot (n_c - 1)}{n_a \cdot n_b \cdot n_c} \cdot \frac{N_A}{MW} = \frac{2ab \cdot (n_c - 1)}{n_c} \cdot \frac{N_A}{MW} \tag{15}$$

where N_A is Avogadro's constant of 6.022×10^{23} mol^{-1}, n_c is the stacking number of individual TOT layers per particle (Fig. 1(b)). In montmorillonites, the count of stacked clay layers n_c depends on the hydration conditions, and a value of 10 is usually assumed under saturated conditions (Delage et al., 2006). MW represents the molar mass of a montmorillonite unit cell (g/mol). A typical structural form of Na-montmorillonite is $Na_{0.6}[Si_{7.8}Al_{0.2}]^{IV}[Al_{3.6}Mg_{0.4}]^{VI}O_{20}(OH)_4$, and therefore, a value of 735 g/mol is employed for MW.

The other variable in Eq. (14), i.e., the interlayer distance h_{in}, can be determined through

XRD measurements. For saturated Kunipia-F clay (99% Na-montmorillonite) compacted at dry densities ranging from 1 to 1.8 g/cm^3, Kozaki et al. (1998) noted that 3-layer hydrates occupy the interlayer space at dry densities below 1.3 g/cm^3. For dry densities exceeding 1.6 g/cm^3, a 2-layer hydrated structure was identified, and both the hydration states will coexist within the density range of 1.3 g/cm^3 to 1.6 g/cm^3. Muurinen et al. (2004) used small angle X-ray scattering (SAXS) to measure purified sodium MX-80 bentonite specimens. They observed an interlayer distance ranging from approximately 0.55 to 1 nm with the dry density decreased from 1.7 to 0.7 g/cm^3. Based on these experimental data, Appelo (2013) suggested the following linear relationship between interlayer distance and the partial dry density of montmorillonite:

$$h_{in} = 1.41 \times 10^{-9} - 4.9 \times 10^{-10} \frac{\rho_{m-partial}}{\rho_w} \tag{16}$$

where $\rho_{m\text{-}partial}$ and ρ_w represent the partial dry density of montmorillonite and pore water density, respectively. Here, $\rho_{m\text{-}partial}$ is defined as the ratio of the dry mass of montmorillonite to the combined volume of montmorillonite minerals and void space:

$$\rho_{m-partial} = \frac{m_m}{V_m + V_v} \tag{17}$$

$\rho_{m\text{-}partial}$ is typically lower than the dry density of specimen ρ_d due to the presence of non-montmorillonite minerals. For the bentonite-sand mixture compositions shown in Fig. 2, Eq. (18) can be derived to calculate $\rho_{m\text{-}partial}$ by combining Eqs. (8)~(12) and Eq. (17):

$$\rho_{m-partial} = \frac{\rho_d \cdot \omega_1 \cdot \alpha}{1 - \left[(1-\alpha) \cdot \frac{\rho_d}{\rho_{sand}} + (1-\omega_1) \cdot \alpha \cdot \frac{\rho_d}{\rho_{nm}} \right]} \tag{18}$$

Assuming the clay mineral is homogeneous and its basal surfaces are perfectly parallel, the adsorbed water volume V_{in} (m^3) is calculated by substituting Eqs. (15) and (16) into Eq. (14):

$$V_{in} = \frac{abh_{in}(n_c - 1)}{n_c} \cdot \frac{N_A}{MW} \cdot m_s \omega \tag{19}$$

The adsorptive water porosity ϕ_{ad} can be determined based on the adsorbed water volume V_{in} as follows:

$$\phi_{ad} = \frac{V_{in}}{m_s / \rho_d} = \frac{abh_{in}\rho_d (n_c - 1)}{n_c} \cdot \frac{N_A}{MW} \cdot \omega \tag{20}$$

Similarly, the capillary water void ratio e_{ca} can be calculated as follows:

$$e_{ca} = e - \frac{V_{in}}{m_s / \rho_s} = e - \frac{abh_{in}(n_c - 1)}{n_c} \cdot \frac{N_A}{MW} \cdot \omega \rho_s \tag{21}$$

where e is the overall void ratio.

3.2 Reduced surface area of void space containing capillary water

Meanwhile, the determination of SSA_{ca} requires the total specific surface area of bentonite-based materials SSA_s, including montmorillonite and non-montmorillonite minerals. Specific surface area of montmorillonite SSA_{Mt} (m^2/g) consists of the internal basal surface area A_{in} and external surface area A_{ex} per unit mass (Fig. 1(b)). Similar to the calculation of A_{in} in Eq. (15), A_{ex} can also be determined based on the crystallographic information of the montmorillonite unit cell as follows (Tournassat and Appelo, 2011):

$$A_{ex} = 2\frac{(n_a a \cdot n_c c^*) + (n_b b \cdot n_c c^*) + (n_a a \cdot n_b b)}{n_a \cdot n_b \cdot n_c} \cdot \frac{N_A}{MW} \tag{22}$$

where n_a and n_b are the stacking number of unit cells along the a and b directions. Commonly, the stacking numbers of n_c are relatively small as compared to n_a and n_b. Consequently, Eq. (22) can be simplified to Eq. (23) and SSA_{Mt} is given by Eq. (24) (Tournassat and Appelo, 2011):

$$A_{ex} = \frac{2a \cdot b}{n_c} \cdot \frac{N_A}{MW} \tag{23}$$

$$SSA_{Mt} = A_{ex} + A_{in} = 2a \cdot b \frac{N_A}{MW} \tag{24}$$

Based on Eq. (24), the specific surface area of Na-montmorillonite SSA_{Mt}, calculated from its crystal structure, is 776 m^2/g. This value is consistent with the typical range of 720-790 m^2/g reported in literature (Tournassat and Appelo 2011; Tournassat et al. 2015). Additionally, the accessory minerals that constitute bentonite are primarily quartz, feldspar, and calcite. The specific surface areas of these accessory minerals are dependent on their particle size distribution. Holmboe et al. (2012) suggested that accessory minerals have a minor effect on the total surface area and approximated their specific surface area as 10 m^2/g. Similarly, Komine and Ogata (1996, 2004) argued that non-swelling minerals in bentonite exhibit significantly lower specific surface areas compared to montmorillonite and assigned a value of 0 m^2/g to these accessory minerals. By assigning these two values (0 or 10 m^2/g) to the non-montmorillonite minerals in bentonite-based materials, the contribution of SSA_{Mt} to SSA_s can be calculated. As depicted in Fig. 3, for ω higher than about 10% (a condition typically satisfied by bentonite-based materials), the proportion of SSA_{Mt} to SSA_s consistently exceeds 90%. Therefore, surface areas of these non-montmorillonite minerals in bentonite-based materials are negligible and $SSA_s = SSA_{Mt} \cdot \omega$ is assumed in this study.

As mentioned above, SSA_{ca}, denoting only a portion of the total specific surface area SSA_s, specifically accounts for the surface area of capillary water voids. Considering that in a densely compacted specimen, where the majority of porosity is confined to the interlayers of montmorillonite, the ratio of SSA_{ca} to SSA_s tends towards 0, signifying an absence of water flow. With increasing the specimen porosity, volume of capillary water pores gradually increases, leading to an increase in the ratio of SSA_{ca} to SSA_s. Meanwhile, in the scenario of very loose bentonite, nearly all the water within the specimen exists as capillary water, and the ratio between the two parameters converges towards 1. Therefore, this study proposes the following relationship among the parameters of SSA_{ca}, SSA_s, and ϕ:

$$SSA_{ca} = SSA_s \cdot \phi^n = SSA_{Mt}\omega \cdot (\frac{e}{e+1})^n \tag{25}$$

where n is a fitted parameter ($n > 0$), which is closely related to the mass fraction of montmorillonite in bentonite clays. According to relationship between the total specific surface area SSA_s and the reduced specific surface area SSA_{ca} illustrated in Eq. (25), SSA_{ca}/SSA_s always increases with the increase in the void ratio. At the same void ratio, a higher n value will result in a lower SSA_{ca}.

Finally, by incorporating the capillary water void ratio e_{ca} calculated by Eq. (21) and the reduced specific surface area SSA_{ca} obtained from Eq. (25) into Eq. (7), the modified KC equation for bentonite-based materials can be given by:

$$K_s = (\frac{1}{C_{K-C}}) \cdot (\frac{\gamma}{\mu}) \cdot (\frac{1}{\rho_s^2 SSA_{Mt}{}^2 \omega^2}) \cdot \frac{e_{ca}{}^3}{e^{2n}(1+e)^{1-2n}} \tag{26}$$

The expression for K_s in Eq. (26) is similar to that proposed by Mbonimpa et al. (2002), who developed analogous expressions for saturated hydraulic conductivity functions in clay soils. Specifically, Mbonimpa et al. (2002) indirectly modified the KC equation by incorporating an additional parameter, the liquid limit, to account for the influence of physico-chemical factors and the "plate-like" structure of clay minerals. In contrast, this study directly modifies the KC equation by distinguishing between voids containing capillary water and those containing adsorptive water. The void ratio and surface area associated with adsorptive water voids were explicitly excluded, focusing solely on the contribution of capillary water to K_s. A detailed comparison of the performance of the Mbonimpa et al. (2002) model and Eq. (26) will be provided later.

4. Unsaturated hydraulic conductivity of bentonite-based materials

For the calculation of the saturated hydraulic conductivity, the contributions of interlayer water to water flow were neglected, since water molecules are strongly adsorbed to the inner basal surface of montmorillonite and has very limited mobility compared to capillary water (Pusch and Yong, 2006). However, under unsaturated conditions, especially in high-suction scenarios, the predominant water type in bentonite-based materials is adsorbed water (Romero et al., 2011; Lu, 2016). In such cases, contributions from adsorbed water should be taken into consideration for the calculation of relative hydraulic conductivity at all suctions.

In this work, a SWRC model was first proposed based on the microstructure of montmorillonite. This SWRC model can describe both the capillarity-dominated regime at low suction ranges and adsorptive-dominated regime at high suction ranges. By integrating this new SWRC into Mualem's (1976) conductivity function, the relative hydraulic conductivity of bentonite-based materials can be determined across the entire range of matric suctions.

4.1 Soil-water retention curve

In this study, the SWRC is expressed by a piecewise function, delineating distinct capillarity-dominated and adsorption-dominated processes, demarcated by a critical matric suction ψ_{cri}. For suctions below ψ_{cri}, the relationship between suction and saturation is primarily governed by capillary processes and can be aptly described by the van Genuchten equation (1980), while adsorption processes mainly dominate at matric suctions higher than ψ_{cri}.

Determining the adsorption-dominated SWRC requires experimental data on the soil water adsorption isotherm, which represents the relationship between the adsorbed water content and the relative humidity. The experimental data of the water vapor sorption isotherms for bentonite materials measured by Akin and Likos (2014) is presented in Fig. 4. While the experimental data from Akin and Likos (2014) reflect total moisture content, which encompasses both capillary moisture (resulting from capillary condensation on particle surfaces and interfaces) and adsorbed moisture, the measured adsorbed water content, depicted as the data point in Fig. 4, is primarily attributed to water adsorption on the large specific surface area of montmorillonite. As illustrated in Fig. 4, the measured adsorbed water content increases slowly with rising relative humidity at first, but the rate of increase accelerates as relative humidity continues to rise.

This study introduces a new mathematical formulation to represent the soil water adsorption isotherm shown in Fig. 4:

$$w_a = w_{a\_\max} \cdot \left\{ 1 - \frac{\ln\left[A \cdot \ln(\mathrm{RH}) \right]}{\ln B} \right\} \quad \mathrm{RH} \in (0,1) \tag{27}$$

where w_a denotes the adsorbed water content, $w_{a\_\max}$ represents the maximum adsorbed water content, RH is the relative humidity, A (< 0) and B (> 1) are two dimensionless parameters that characterize the shape of the curve. In Fig. 4, the dots represent the experimental results, while the solid lines correspond to the calculations from Eq. (27). The fitting results demonstrate good agreement with the measured isotherms for different bentonite soils.

Applying Kelvin's equation (Eq. (28)) to Eq. (27), the adsorbed volume can be rearranged as a function of suction ψ as:

$$\psi = -\frac{RT}{V_{mw}} \cdot \ln(\mathrm{RH}) \tag{28}$$

$$\frac{w_a}{w_{a\_\max}} = 1 - \frac{\ln(C \cdot \psi)}{\ln B} \tag{29}$$

Where R is the gas constant, T is temperature, V_{mw} is the partial molar volume of the water vapour, and $C = -A \cdot V_{mw}/RT$. Eq. (29) indicates that the adsorbed water volume will consistently increase with decreasing the matric suction. When the matric suction is equal to $1/C$, the adsorbed water content reaches its maximum value of $w_{a\_\max}$. Below this suction, any additional water molecules will transition into capillary water. Therefore, let $\psi_{cri} = 1/C$ be the delamination of the adsorption- and capillarity-dominated processes, a more general form of Eq. (29) can be proposed for bentonite materials as follows:

$$\frac{S}{S_{ad}} = 1 - \frac{\ln(\psi / \psi_{cri})}{\ln B} \tag{30}$$

where S represents the water saturation. S_{ad} is the maximum adsorbed saturation at $\psi = \psi_{cri}$ and its value can be determined based on Eq. (20):

$$S_{ad} = \frac{\phi_{ad}}{\phi} = \frac{abh_{in}(n_c - 1)}{n_c} \cdot \frac{N_A}{MW} \cdot \frac{\omega \rho_d}{\phi} \tag{31}$$

Combined with the VG equation (van Genuchten, 1980), the proposed SWRC function is given by:

$$S = \begin{cases} [1+(\frac{\psi}{\psi_a})^m]^{(1-m)/m} & \text{for } 0 \le \psi \le \psi_{cri} \\ S_{ad} \cdot \left[1 - \frac{\ln(\psi / \psi_{cri})}{\ln B}\right] & \text{for } \psi \ge \psi_{cri} \end{cases} \tag{32}$$

where ψ_a and m are model parameters of the VG equation. It is important to note that the assumption of water configuration within bentonite-based materials, in which adsorbed water and capillary water occur successively as matric suction decreases, represents a simplified approximation for developing the SWRC model. This simplified framework may not fully reflect actual observations, as the coexistence of water in interlayer spaces and larger pores is possible due to the thermodynamic equilibrium that is always maintained between water in these regions. This phenomenon is further supported by Fernández and Villar (2010), who indirectly observed such coexistence even at extremely high suction levels. Therefore, the proposed SWRC model should be interpreted as an idealized scenario rather than a complete description of water retention behavior in bentonite-based materials.

Ensuring the continuity of the proposed SWRC equation involves equating the two segments of the Eq. (32) at the critical suction point ψ_{cri}. Meanwhile, in order to make the SWRC smooth, an additional relationship can be established by setting the first-order derivatives of the two segments of the function equal. Based on these two relationships, two out of the four unknown parameters in Eq. (32) (ψ_{cri}, B, ψ_a and m) can be determined. Here, B and ψ_a are explicitly expressed as analytical functions of ψ_{cri} and m:

$$B = \exp\left[\frac{1}{(1-S_{ad}{}^{m/(m-1)})\cdot(m-1)}\right] \tag{33}$$
$$\psi_a = \psi_{cri}\cdot\left[S_{ad}{}^{m/(1-m)}-1\right]^{-1/m}$$

By substituting Eq. (33) into Eq. (32), only two parameters, ψ_{cri} and m, are left. These values are subsequently optimized through regression analysis on experimental data.

4.2 Calculation of unsaturated hydraulic conductivity

Equation (32) introduces a new soil-water retention function that encompasses both capillarity-dominated and adsorption-dominated processes. This proposed SWRC equation can be expressed in closed form, making it compatible for integration into the conductivity model of Mualem (1976). In the following sections, we will derive an analytical solution for K_r at all matric suctions specific to bentonite-based materials.

Mualem (1976)'s model for calculation of relative hydraulic conductivity K_r is:

$$K_r(S) = S^{1/2}\left[\int_0^S dS/\psi \Big/ \int_0^1 dS/\psi\right]^2 \tag{34}$$

Solving this equation for $\psi = \psi(S)$ and substituting the resulting expression into Eq. (34) gives:

$$K_r(S) = S^{1/2}\left[\Gamma(S)/\Gamma(1)\right]^2 \tag{35}$$

where

$$\Gamma(S) = \int_0^S \frac{1}{\psi(S)}dS \tag{36}$$

Applying the two portions of Eq. (32) to Eq. (36), one obtains:

$$\Gamma_{\mathrm{I}}(S) = \int_{S_{ad}}^{S}\frac{1}{\psi_a}\cdot(S^{\frac{m}{1-m}}-1)^{-\frac{1}{m}}dS = \frac{1}{\psi_a}\cdot\left[(1-S_{ad}{}^{\frac{m}{m-1}})^{\frac{m-1}{m}}-(1-S^{\frac{m}{m-1}})^{\frac{m-1}{m}}\right] \text{ for } S \ge S_{ad} \tag{37}$$

$$\Gamma_{\mathrm{II}}(S) = \int_0^S \frac{1}{\psi_{cri}}\cdot B^{(\frac{S}{S_{ad}}-1)}dS = \frac{1}{\psi_{cri}}\cdot\frac{S_{ad}}{\ln B}(B^{\frac{S}{S_{ad}}-1}-B^{-1}) \text{ for } 0 \le S \le S_{ad} \tag{38}$$

Again, S_{ad} signifies the maximum adsorption saturation at ψ_{cri}, and its value can be determined using Eq. (31). Combining Eqs. (37) and (38) give the integral for any value of S:

$$\Gamma(S) = \Gamma_{\mathrm{I}}(S) + \Gamma_{\mathrm{II}}(S_{ad}) \quad \text{for } S \geq S_{ad} \tag{39}$$

$$\Gamma(S) = \Gamma_{\mathrm{II}}(S) \quad \text{for } 0 \leq S \leq S_{ad} \tag{40}$$

The total integral from $S = 0$ to 1 is:

$$\Gamma(1) = \Gamma_{\mathrm{I}}(1) + \Gamma_{\mathrm{II}}(S_{ad}) \tag{41}$$

Combining Eqs. (35), (39), (40) and (41) give analytical solutions to K_r:

$$\begin{aligned} K_r(S) &= S^{1/2}\left[\frac{\Gamma_{\mathrm{I}}(S) + \Gamma_{\mathrm{II}}(S_{ad})}{\Gamma_{\mathrm{I}}(1) + \Gamma_{\mathrm{II}}(S_{ad})}\right]^2 \quad \text{for } S \geq S_{ad} \\ K_r(S) &= S^{1/2}\left[\frac{\Gamma_{\mathrm{II}}(S)}{\Gamma_{\mathrm{I}}(1) + \Gamma_{\mathrm{II}}(S_{ad})}\right]^2 \quad \text{for } 0 \leq S \leq S_{ad} \end{aligned} \tag{42}$$

Combined with K_s determined through Eq. (26), the unsaturated hydraulic conductivity of bentonite-based materials at any saturation can be determined.

5. Verification and discussion

In this study, only three parameters are involved in the equations for saturated and relative hydraulic conductivity. Parameter n is associated with the saturated hydraulic conductivity equation, while ψ_{cri} and m pertain to the relative hydraulic conductivity equations. The parameter n is calibrated by fitting Eq. (26) to the experimental data of hydraulic conductivity obtained from saturated water flow tests on bentonite-based specimens. The parameters ψ_{cri} and m are calibrated using experimental results from water retention tests, where Eq. (32) is fitted to the effective saturation and matric suction data points. With the obtained values of ψ_{cri} and m, the relative hydraulic conductivity is computed using Eq. (42). Subsequently, based on the saturated and relative hydraulic conductivities calculated, unsaturated hydraulic conductivity can be determined and evaluated against experimental data.

5.1 Model evaluation for saturated hydraulic conductivity

To validate the modified KC equation (Eq. (26)), experimental results of K_s on different types of bentonites and bentonite-sand mixtures are collected. Tables 1 and 2 provide detailed information about the bentonite-based materials. The least squares method is employed to determine the parameter n in Eq. (26) by fitting the dataset of hydraulic conductivity and void ratio. Once the n value is determined, the hydraulic conductivity can be calculated and compared with the experimentally measured values.

Figs. 5 and 6 present comparisons of the K_s of bentonites and bentonite-sand mixtures, as calculated by the conventional KC equation and the modified form proposed in this study (Eq. (26)). In Fig. 5, calculation results from an additional model, the Mbonimpa et al. (2002) model, are also included. As shown in Fig. 5, the conventional KC model show obvious deviations from the measured K_s data for bentonites. For bentonite-sand mixtures, the conventional KC model either significantly overestimates (Fig. 6(a)) or underestimates (Fig. 6(b)) the K_s values. The Mbonimpa et al. (2002) model shows good predictions for most bentonite specimens, but tends to overestimate the K_s of FEBEX and Kunibond bentonite specimens, as illustrated in Fig. 5. In contrast, the modified KC model with optimized n value shows good agreement with the experimental data. The model-calculated curve closely aligns with the experimental data points for both bentonites and bentonite-sand mixtures. Meanwhile, a quantitative comparison between the calculated hydraulic conductivity by the modified KC model and the experimental data is depicted in Fig. 7. Results in Fig. 7 reveal that the majority of calculated hydraulic conductivity values fall within the range of 1/3 to 3 times the measured values. This is within the anticipated typical range of experimental errors, confirming the validity and accuracy of the modified KC equation in calculating hydraulic conductivity for both bentonite and bentonite-sand mixtures.

Given that the modified KC model incorporates a fitted parameter n, which may impose limitations on the broad applicability of the proposed model. As mentioned above, parameter n represents the proportion of reduced specific surface area SSA_{ca} to the total specific surface area SSA_s, and is closely related to the mass content of montmorillonite in bentonite specimens. Therefore, Fig. 8 establishes the evolution of n value with the mass fraction of montmorillonite ω for the two databases. As can be seen in Fig. 8, the n value increased exponentially with ω and a strong correlation between the parameter n and ω can be characterized for bentonite-based materials as follows:

$$n = 0.806 \cdot \exp(\frac{\omega}{0.6544}) - 0.486 \tag{43}$$

By substituting Eq. (43) into the modified KC equation (Eq. (26)), the K_s can be calculated based on the mass fraction of montmorillonite ω without any fitting parameters. For verification, the hydraulic conductivity, with n value obtained by Eq. (43), is plotted against the experimentally determined values, as depicted in Fig. 9. The graph reveals a notable concordance between the model's determined values and the experimental data, suggesting that employing the ω parameter is sufficient for generating reliable determinations for the hydraulic conductivity of bentonite.

In this study, instead of relying on the overall porosity ϕ and total surface area SSA_s of bentonite, we exclusively utilize the reduced specific surface area SSA_{ca} and porosity ϕ_{ca}, corresponding to the contributions of only capillary water. In Fig. 10, the evolution of SSA_{ca}/SSA_s and ϕ_{ca}/ϕ are illustrated concerning changes in porosity and the mass fraction of montmorillonite. It is evident from Fig. 10 that both the SSA_{ca}/SSA_s and ϕ_{ca}/ϕ will decrease significantly with increasing ω and decreasing the porosity. In the case of bentonite materials with a montmorillonite fraction of 70% and dry density of 1700 kg/m³, only a fraction lower than 0.3 of the total surface area and porosity actively contributes to water flow, as illustrated in Fig. 10. This clarifies why determinations of the K_s by the conventional KC equation tend to deviate from experimental results for bentonite-based materials.

5.2 Unsaturated hydraulic conductivity

5.2.1 Evaluation of SWRC equation

To verify the analytical equations for unsaturated hydraulic conductivity, we first tested the SWRC equation Eq. (32) using experimental data of three types of bentonites reported by Cui et al. (2008), Ye et al. (2012), and Zeng et al. (2022), as listed in Table 3. Due to the lack of saturated water content data in these experimental studies, water content measured at the lowest suction levels (0.1 or 0.01 MPa) is used to represent the saturated water content as an approximation. The water contents were then converted into degrees of saturation. The parameters whose values are determined through the regression analysis are ψ_{cri} and m, while the remaining parameters of B and ψ_a are calculated using Eq. (33). The calibrated parameters are listed in Table 4 and were then applied in Eq. (42) to calculate relative conductivities for the three bentonites. Finally, combined with the saturated hydraulic conductivity K_s, unsaturated hydraulic conductivity can be computed and evaluated against the experimental data. Note that, in contrast to the extensive research on the K_s of bentonite-based materials, studies on the relative hydraulic conductivity under unsaturated conditions are very limited due to experimental difficulties. The experimental data of unsaturated hydraulic conductivity are also sourced from Cui et al. (2008), Ye et al. (2012), and Zeng et al. (2022), and the tested specimens have the same specifications as the water retention tests. The values of K_s for the calculating of unsaturated hydraulic conductivity were estimated based on Eq. (26) or directly obtained from literature to ensure an optimal fit. For comparative analysis, we also conducted evaluations using the original van Genuchten equation to fit all of the SWRC data.

Fig. 11 shows the calculated and measured SWRC data of three types of bentonites. As depicted in the graphs, the fitting for the three bentonites is generally good for both Eq. (32) and the original VG equation. Notably, the model-calculated curves based on the two equations nearly coincide with each other within the suction range examined in the SWRC data. Subsequently, Eq. (32) exhibits a noticeable deviation from the VG equation, declining more rapidly to zero water saturation. For the model-calculated results from Eq. (32), the matric suctions at zero water saturation are 2395, 2001 and 1287 MPa for Kunigel-V1 bentonite/sand mixture, GMZ bentonite and MX-80 bentonite/Cox claystone mixture, respectively. However, the fitting results using the original VG model indicate that the water saturation at suction of 1000 MPa is still around 0.2 for the three bentonite-based soils, which is physically unrealistic. Although VG model can provide a continuous and smooth SWRC across the entire suction range, its derivations are determined by the shape of the SWRC rather than the underlying water-retention mechanisms (Lu, 2016). This may result in calculating errors when applied in conductivity models, especially for bentonite-based materials, where significant amounts of adsorbed water can coexist with capillary water.

5.2.2 Evaluation of unsaturated hydraulic conductivity

Fig. 12 presents the model-calculated results of the three types of bentonite soils based on Eq. (42) and the original van Genuchten-Mualem (VG-M) model. Obviously, the calculated hydraulic conductivity based on Eq. (42) shows good agreement with the experimental results, while the VG-M model can underestimate the unsaturated hydraulic conductivity by up to three orders of magnitude. The VG equation, by not allowing water saturation to reduce to zero within a finite suction, as presented in Fig. 11, leads to an overestimation of the term $\Gamma(1)$ in Eq. (35) and ultimately results in an underestimation of the unsaturated hydraulic conductivity.

As a test, an analysis is conducted with S_{ad} set as a fitted parameter to investigate whether this analytical equation can be applicable in situations where determining the adsorbed water volume is challenging or for non-bentonite-based materials. The resulting parameters are summarized in Table 5, and these values did not show a significant difference from the results with S_{ad} calculated by Eq. (31), as listed in Table 4. Based on the obtained parameters in Tables 4 and 5, the relative hydraulic conductivity can be determined using Eq. (42). Evolution of the calculated relative hydraulic conductivity with degree of saturation is presented in Fig. 13. The solid and dashed lines in Fig. 13 represent the calculated relative hydraulic conductivity with S_{ad} calculated by Eq. (31) and set as a fitted parameter, respectively. As shown in Fig. 13, the model calculation of relative hydraulic conductivity using parameters in Table 5 also exhibited a minor difference from the case with S_{ad} calculated by Eq. (31), especially for Kunigel-V1/sand mixture and MX-80 bentonite/Cox claystone mixture. Without tests against more reliable data, caution is still advised since the accuracy of the proposed equations, particularly when setting S_{ad} as a fitted parameter in scenarios involving non-bentonite-based clays, is not known.

6. Conclusion

This study proposed equations for describing the hydraulic properties of bentonite-based materials with consideration of microstructure and crystallographic information of montmorillonite.

For the saturated hydraulic conductivity, modifications to the Kozeny-Carman equation were conducted by subtracting the surface area and the void ratio of adsorbed water pores in bentonite. The adsorbed porewater volume was computed by multiplying the internal basal surface with the interlayer distance. Meanwhile, a fitted parameter was introduced to establish the relationship between the reduced and total specific surface areas, and the overall porosity. These parameters were then utilized in accordance with Poiseuille's law to generate the expressions for calculating saturated hydraulic conductivity.

For partially saturated bentonite, the SWRC is expressed by a piecewise function. This function delineates clear distinctions between capillary-dominated and adsorption-dominated processes, demarcated by a critical matric suction. Maximum adsorbed water volume is reached at this critical matric suction. Constraints are imposed on this equation to ensure a continuous derivative and force the function to reach zero water saturation within a finite suction. This SWRC function was utilized with the Mualem model to generate closed-form analytical expressions in calculating relative hydraulic conductivity.

The proposed equations were verified using the experimentally measured data from a diverse range of bentonite types and bentonite-sand mixtures. For bentonite-based materials with montmorillonite mass fractions below 10%, the model calculations exhibited good agreement with the measured data, confirming the validity of these analytical expressions in accurately calculating the hydraulic properties of bentonite-based soils.

Acknowledgements

The financial supports of the National Nature Science Foundation of China (42030714 and 42202304) are greatly acknowledged. This work is also supported by the Shenzhen Science and Technology Innovation Commission through grant 2022N040.

Notation

A, B	fitting parameters controlling the shape of adsorption isotherm curve
A_{in}	internal basal surface area per unit mass of montmorillonite
A_{ex}	external surface area of montmorillonite per unit mass
a	dimension of montmorillonite unit cell in a-direction
b	dimension of montmorillonite unit cell in b-direction
C	parameter with a value of $-A \cdot V_{mw}/RT$
c	dimension of montmorillonite unit cell in c-direction
c^*	the orthogonally projected c-axis of the montmorillonite unit cell
$C_{K\text{-}C}$	Kozeny constant
e	overall void ratio
e_{ca}	void ratio of pores containing capillary water
h_{in}	interlayer distance
K	hydraulic conductivity at a given saturation state
k	shape factor

K_r	relative hydraulic conductivity
K_s	saturated hydraulic conductivity
L_e	actual channel length
L	specimen length
m_s	dry mass of bentonite-based materials
m_m	dry mass of montmorillonite in the bentonite
m_{nm}	dry mass of minerals excluding montmorillonite in bentonite
m_{sand}	dry mass of sand in bentonite-sand mixtures
MW	molar mass of a montmorillonite unit cell
n	fitting parameter
N_A	Avogadro's constant
n_a	number of unit cells stacked for a montmorillonite particle in *a*-direction
n_b	number of unit cells stacked for a montmorillonite particle in *b*-direction
n_c	number of unit cells stacked for a montmorillonite particle in *c*-direction
R	gas constant
RH	relative humidity
R_h	hydraulic radius
S	water saturation
S_{ad}	maximum adsorbed saturation at $\psi = \psi_{cri}$
SSA_{ca}	reduced specific surface area
SSA_{Mt}	specific surface area of montmorillonite
SSA_s	specific surface area of bentonite-based materials
T	temperature
V	apparent velocity through a porous medium
V_m	volume of montmorillonite mineral in bentonite
V_{nm}	volume of minerals excluding montmorillonite in bentonite
V_{sand}	volume of sand
V_v	volume of the void space in the bentonite-based materials
v	actual velocity in the pores
V_{in}	interlayer or adsorbed water volume
V_{mw}	partial molar volume of water vapour
w_a	adsorbed water content
$w_{a\_\max}$	maximum adsorbed water content
α	mass content of bentonite in bentonite-sand mixtures
ρ_d	dry density of bentonite
ρ_w	dry density of pore water
$\rho_{m\text{-}partial}$	partial dry density of montmorillonite
ρ_s	density of the soil particle
ρ_m	particle density of montmorillonite
ρ_{nm}	particle density of constituent minerals other than montmorillonite within the bentonite
ρ_{sand}	particle density of sand

γ	unit weight of capillary water
μ	viscosity of capillary water
ψ_{cri}	critical matric suction
ψ	suction
ψ_a, m	model parameters of the VG equation
ω	mass content of montmorillonite in bentonite-sand mixtures
ω_1	mass content of montmorillonite in bentonites
ϕ	overall porosity of the porous medium
ϕ_{ad}	adsorptive water porosity

References

Akin, I.D., and Likos, W.J. 2014. Specific surface area of clay using water vapor and EGME sorption methods. Geotechnical Testing Journal, **37**(6): 1016-1027. https://doi.org/10.1520/GTJ20140064.

Alyamani, M.S., and Şen, Z. 1993. Determination of hydraulic conductivity from complete grain-size distribution curves. Groundwater **31**(4): 551-555. https://doi.org/10.1111/j.1745-6584.1993.tb00587.x.

Appelo, C. 2013. A review of porosity and diffusion in bentonite. Posiva Oy (No. POSIVAWR-13-29, Olkiluoto, pp. 1-11).

Aubertin, M., Mbonimpa, M., Bussière, B., and Chapuis, R.P. 2003. A model to predict the water retention curve from basic geotechnical properties. Canadian Geotechnical Journal, **40**(6): 1104-1122. https://doi.org/10.1139/t03-054.

Bourg, I.C., Bourg, A.C., and Sposito, G. 2003. Modeling diffusion and adsorption in compacted bentonite: a critical review. Journal of Contaminant Hydrology, **61**(1-4): 293-302. https://doi.org/10.1016/S0169-7722(02)00128-6.

Bourg, I.C., Sposito, G., and Bourg, A. 2006. Tracer diffusion in compacted, water-saturated bentonite. Clays and Clay Minerals, **54**(3): 363-374. https://doi.org/10.1346/CCMN.2006.0540307.

Bradbury, M.H., and Baeyens, B. 2003. Porewater chemistry in compacted re-saturated MX-80 bentonite. Journal of Contaminant Hydrology, **61**(1-4): 329-338. https://doi.org/10.1016/S0169-7722(02)00125-0.

Carman, P.C. 1937. Fluid flow through a granular bed. Transactions of the Institution of Chemical Engineers, **15**: 150-156.

Carrier III, W.D. 2003. Goodbye, Hazen; Hello, Kozeny-Carman. Journal of Geotechnical and Geoenvironmental Engineering, **129**(11): 1054-1056. https://doi.org/10.1061/(ASCE)1090-0241(2003)129:11(1054).

Chapuis, R.P. 2002. The 2000 RM Hardy Lecture: Full-scale hydraulic performance of soil bentonite and compacted clay liners. Canadian Geotechnical Journal, **39**(2): 417-439. https://doi.org/10.1139/t01-092.

Chapuis, R.P., and Aubertin, M. 2003. On the use of the Kozeny Carman equation to predict the hydraulic conductivity of soils. Canadian Geotechnical Journal, **40**(3): 616-628. https://doi.org/10.1139/t03-013.

Chapuis, R.P. 2012. Predicting the saturated hydraulic conductivity of soils: a review. Bulletin of Engineering Geology and the Environment, **71**: 401-434. https://doi.org/10.1007/s10064-012-0418-7.

Chen, T., Sedighi, M., Jivkov, A.P., and Seetharam, S.C. 2021. A model for hydraulic conductivity of compacted bentonite–inclusion of microstructure effects under confined wetting. Géotechnique, **71**(12): 1071-1084. https://doi.org/10.1680/jgeot.19.P.088.

Cui, L.Y., Ye, W.M., Wang, Q., Chen, Y.G., and Cui, Y.J. 2023. A model for describing advective and diffusive gas transport through initially saturated bentonite with consideration of temperature. Engineering Geology, **323**: 107215. https://doi.org/10.1016/j.enggeo.2023.107215.

Cui, L.Y., Ye, W.M., Wang, Q., Chen, Y.G., Chen, B., and Cui, Y.J. 2022. Insights into gas migration in saturated GMZ bentonite using the RCP technique. Engineering Geology, **303**: 106646. https://doi.org/10.1016/j.enggeo.2022.106646.

Cui, L.Y., Ye, W.M., Wang, Q., Chen, Y.G., Chen, B., and Cui, Y.J. 2019. Investigation on gas migration in saturated bentonite using the residual capillary pressure technique with consideration of temperature. Process Safety and Environmental Protection, **125**: 269-278. https://doi.org/10.1016/j.psep.2019.03.036.

Cui, Y.J., Tang, A.M., Loiseau, C., and Delage, P. 2008. Determining the unsaturated hydraulic conductivity of a compacted sand-bentonite mixture under constant-volume and free-swell conditions. Physics and Chemistry of the Earth, Parts A/B/C, **33**: S462-S471. https://doi.org/10.1016/j.pce.2008.10.017.

Delage, P., Marcial, D., Cui, Y.J., and Ruiz, X. 2006. Ageing effects in a compacted bentonite: a microstructure approach. Géotechnique, **56**(5): 291-304. https://doi.org/10.1680/geot.2006.56.5.291.

Dixon, D.A., Graham, J., Gray, M.N. 1999. Hydraulic conductivity of clays in confined tests under low hydraulic gradients. Canadian Geotechnical Journal, **36**(5): 815-825. https://doi.org/10.1139/t99-057.

Fayer, M.J., and Simmons, C.S. 1995. Modified soil water retention functions for all matric suctions. Water Resources Research, **31**(5), 1233-1238. https://doi.org/10.1029/95WR00173.

Fernández, A.M., and Villar, M.V. 2010. Geochemical behaviour of a bentonite barrier in the laboratory after up to 8 years of heating and hydration. Applied Geochemistry, **25**(6): 809-824. https://doi.org/10.1016/j.apgeochem.2010.03.001.

Holmboe, M., Wold, S., and Jonsson, M. 2012. Porosity investigation of compacted bentonite using XRD profile modeling. Journal of Contaminant Hydrology, **128**(1-4): 19-32. https://doi.org/10.1016/j.jconhyd.2011.10.005.

Ito, D., Wang, H., and Komine, H. 2022. Hydraulic conductivity test system for compacted, 2-mm-thick bentonite specimens. Soils and Foundations, **62**(5): 101210. https://doi.org/10.1016/j.sandf.2022.101210.

Karnland, O., Nilsson, U., Weber, H., and Wersin, P. 2008. Sealing ability of Wyoming bentonite pellets foreseen as buffer material–Laboratory results. Physics and Chemistry of the Earth, Parts A/B/C, **33**: S472-S475. https://doi.org/10.1016/j.pce.2008.10.024.

Koltermann, C.E., and Gorelick, S.M. 1995. Fractional packing model for hydraulic conductivity derived from sediment mixtures. Water Resources Research, **31**(12): 3283-3297. https://doi.org/10.1029/95WR02020.

Komine, H. 2021. Cation filtration of montmorillonite on hydraulic conductivities of some bentonites in artificial seawater. Journal of Geotechnical and Geoenvironmental Engineering, **147**(5): 06021002. https://doi.org/10.1061/(ASCE)GT.1943-5606.0002513.

Komine, H. 2008. Theoretical equations on hydraulic conductivities of bentonite-based buffer and backfill for underground disposal of radioactive wastes. Journal of Geotechnical and Geoenvironmental Engineering, **134**(4): 497-508. https://doi.org/10.1061/(ASCE)1090-0241(2008)134:4(497).

Komine, H. 2004. Simplified evaluation on hydraulic conductivities of sand-bentonite mixture backfill. Applied Clay Science, **26**(1-4): 13-19. https://doi.org/10.1016/j.clay.2003.09.006.

Komine, H., and Ogata, N. 2004. Predicting swelling characteristics of bentonites. Journal of Geotechnical and Geoenvironmental Engineering, **130**(8): 818-829. https://doi.org/10.1061/(ASCE)1090-0241(2004)130:8(818)

Komine, H., and Ogata, N. 1996. Prediction for swelling characteristics of compacted bentonite. Canadian geotechnical journal, **33**(1), 11-22. https://doi.org/10.1139/t96-021.

Kozaki, T., Inada, K., Sato, S., and Ohashi, H. 2001. Diffusion mechanism of chloride ions in sodium montmorillonite. Journal of Contaminant Hydrology, **47**(2-4): 159-170. https://doi.org/10.1016/S0169-7722(00)00146-7.

Kozaki, T., Fujishima, A., Sato, S., and Ohashi, H. 1998. Self-diffusion of sodium ions in compacted sodium montmorillonite. Nuclear Technology, **121**(1): 63-69. https://doi.org/10.13182/NT98-A2819.

Kozeny, J. 1927. Ueber kapillare leitung des wassers im boden. Sitzungsberichte der Akademie der Wissenschaften in Wien, **136**: 271.

Lebeau, M., and Konrad, J.M. 2010. A new capillary and thin film flow model for predicting the hydraulic conductivity of unsaturated porous media. Water Resources Research, **46**(12). https://doi.org/10.1029/2010WR00909.

Liu, J.F., Skoczylas, F., and Talandier, J. 2015. Gas permeability of a compacted bentonite–sand mixture: coupled effects of water content, dry density, and confining pressure. Canadian Geotechnical Journal, 52(8): 1159-1167. https://doi.org/10.1139/cgj-2014-0371.

Liu, J.F., Davy, C.A., Talandier, J., and Skoczylas, F. 2014. Effect of gas pressure on the sealing efficiency of compacted bentonite-sand plugs. Journal of Contaminant Hydrology, 170: 10-27. https://doi.org/10.1016/j.jconhyd.2014.09.006.

Lloret, A., and Villar, M.V. 2007. Advances on the knowledge of the thermo-hydro-mechanical behaviour of heavily compacted “FEBEX” bentonite. Physics and Chemistry of the Earth, Parts A/B/C, **32**(8-14): 701-715. https://doi.org/10.1016/j.pce.2006.03.002.

Lu, N. 2016. Generalized soil water retention equation for adsorption and capillarity. Journal of Geotechnical and Geoenvironmental Engineering, **142**(10): 04016051. https://doi.org/10.1061/(ASCE)GT.1943-5606.0001524.

Lukasiewicz, S.J., and Reed, J.S. 1988. Specific permeability of porous compacts as described by a capillary model. Journal of the American Ceramic Society, **71**(11): 1008-1014. https://doi.org/10.1111/j.1151-2916.1988.tb07572.x.

Madsen, F.T. 1998. Clay mineralogical investigations related to nuclear waste disposal. Clay minerals, **33**(1): 109-129. https://doi.org/10.1180/000985598545318.

Mbonimpa, M., Aubertin, M., Chapuis, R.P., and Bussière, B. 2002. Practical pedotransfer functions for estimating the saturated hydraulic conductivity. Geotechnical & Geological Engineering, **20**: 235-259. https://doi.org/10.1023/A:1016046214724.

Mualem, Y. 1976. A new model for predicting the hydraulic conductivity of unsaturated porous media. Water Resources Research, **12**(3): 513-522. https://doi.org/10.1029/WR012i003p00513.

Muurinen, A., Karnland, O., and Lehikoinen, J. 2007. Effect of homogenization on the microstructure and exclusion of chloride in compacted bentonite. Physics and Chemistry of the Earth, Parts A/B/C, **32**(1-7): 485-490. https://doi.org/10.1016/j.pce.2006.02.058.

Muurinen, A., Karnland, O., and Lehikoinen, J. 2004. Ion concentration caused by an external solution into the porewater of compacted bentonite. Physics and Chemistry of the Earth, Parts A/B/C, **29**(1): 119-127. https://doi.org/10.1016/j.pce.2003.11.004.

Ng, C.W., Zhou, C., and Ni, J. 2024a. Advanced Unsaturated Soil Mechanics: Theory and Applications. CRC Press.

Ng, C.W., Qu, C., Guo, H., Chen, R., and Xue, Q. 2024b. Probabilistic analysis of a sustainable landfill cover considering stress-dependent water retention model and copula-based random fields. Engineering Geology, **332**, 107460. https://doi.org/10.1016/j.enggeo.2024.107460.

Ng, C.W., Liu, J., Chen, R., and Xu, J. 2015a. Physical and numerical modeling of an inclined three-layer (silt/gravelly sand/clay) capillary barrier cover system under extreme rainfall. Waste Management, **38**: 210-221. https://doi.org/10.1016/j.wasman.2014.12.013.

Ng, C.W., Liu, J., Chen, R., and Coo, J.L. 2015b. Numerical parametric study of an alternative three-layer capillary barrier cover system. Environmental Earth Sciences, **74**: 4419-4429. https://doi.org/10.1007/s12665-015-4462-z.

Pusch, R., and Yong, R.N. 2006. Microstructure of smectite clays and engineering performance. Taylor & Francis, London and New York.

Revil, A., and Lu, N. 2013. Unified water isotherms for clayey porous materials. Water Resources Research, **49**(9): 5685-5699. https://doi.org/10.1002/wrcr.20426.

Romero, E., Della Vecchia, G., and Jommi, C. 2011. An insight into the water retention properties of compacted clayey soils. Géotechnique, **61**(4): 313-328. https://doi.org/10.1680/geot.2011.61.4.313.

Ruan, K., Komine, H., Ito, D., Miyoshi, K., and Gotoh, T. 2022. Hydraulic conductivity and X-ray diffraction tests of unsaturated bentonites with a multi-ring and their predictions by pores distributions. Engineering Geology, **306**: 106738. https://doi.org/10.1016/j.enggeo.2022.106738.

Rossi, C., and Nimmo, J.R. 1994. Modeling of soil water retention from saturation to oven dryness. Water Resources Research, **30**(3), 701-708. https://doi.org/10.1029/93WR03238.

Suzuki, S., Prayongphan, S., Ichikawa, Y., and Chae, B.G. 2005. In situ observations of the swelling of bentonite aggregates in NaCl solution. Applied clay science, **29**(2): 89-98. https://doi.org/10.1016/j.clay.2004.11.001.

Tournassat, C., and Appelo, C.A.J. 2011. Modelling approaches for anion-exclusion in compacted Na-bentonite. Geochimica et Cosmochimica Acta, **75**(13): 3698-3710. https://doi.org/10.1016/j.gca.2011.04.001.

Tournassat, C., Steefel, C.I., Bourg, I.C., and Bergaya, F. 2015. Natural and engineered clay barriers. Elsevier.

Van Genuchten, M.T. 1980. A closed-form equation for predicting the hydraulic conductivity of unsaturated soils. Soil Science Society of America Journal, **44**(5): 892-898. https://doi.org/10.2136/sssaj1980.03615995004400050002x.

Wang, Q., Cui, Y.J., Tang, A.M., Barnichon, J.D., Saba, S., and Ye, W.M. 2013. Hydraulic conductivity and microstructure changes of compacted bentonite/sand mixture during hydration. Engineering Geology, **164:** 67-76. https://doi.org/10.1016/j.enggeo.2013.06.013.

Wersin, P., Curti, E., and Appelo, C.A.J. 2004. Modelling bentonite–water interactions at high solid/liquid ratios: swelling and diffuse double layer effects. Applied clay science, **26**(1-4): 249-257. https://doi.org/10.1016/j.clay.2003.12.010.

Xiang, G., Ye, W., Xu, Y., and Jalal, F.E. 2020. Swelling deformation of Na-bentonite in solutions containing different cations. Engineering Geology, **277**: 105757. https://doi.org/10.1016/j.enggeo.2020.105757.

Xu, L., Ye, W.M., and Ye, B. 2017. Gas breakthrough in saturated compacted GaoMiaoZi (GMZ) bentonite under rigid boundary conditions. Canadian Geotechnical Journal, **54**(8): 1139-1149. https://doi.org/10.1139/cgj-2016-0220.

Ye, W.M., Wan, M., Chen, B., Chen, Y.G., Cui, Y.J., and Wang, J. 2012. Temperature effects on the unsaturated permeability of the densely compacted GMZ01 bentonite under confined conditions. Engineering Geology, **126**: 1-7. https://doi.org/10.1016/j.enggeo.2011.10.011.

Yoon, S., Kim, M.S., Kim, G.Y., and Lee, S.R. 2021. Contemplation of relative hydraulic conductivity for compacted bentonite in a high-level radioactive waste repository. Annals of Nuclear Energy, **161**: 108439. https://doi.org/10.1016/j.anucene.2021.108439.

Zeng, Z., Cui, Y.J., and Talandier, J. 2022. Investigation of the hydraulic conductivity of an unsaturated compacted bentonite/claystone mixture. Géotechnique, **72**(10): 911-921. https://doi.org/10.1680/jgeot.20.P.321.

Figure captions

Fig. 1. Schematic diagram of microstructure and water types in bentonite-based materials (modified after Bradbury and Baeyens, 2003; Tournassat et al., 2015): (a) TOT layer and unit cell of montmorillonite, (b) formation of montmorillonite particle, and (c) water distribution.

Fig. 2. Composition of bentonite-sand mixture and definition of the density of the soil particle ρ_s and partial dry density of montmorillonite $\rho_{m\text{-}partial}$.

Fig. 3. Contributions of SSA_{Mt} to total SSA_s of bentonite. Subscript '*ac*' represents the non-montmorillonite minerals in bentonite-based materials.

Fig. 4. Measured (data point) and predicted (solid line) soil water adsorption isotherms by Eq. (27) for bentonite materials.

Fig. 5. Comparison of prediction saturated hydraulic conductivity for bentonite materials: conventional KC equation, Mbonimpa et al. (2002) model and the modified model of Eq. (26).

Fig. 6. Comparison of predicted saturated hydraulic conductivity for bentonite-sand mixtures: conventional KC equation and the modified model of Eq. (26).

Fig. 7. The predicted saturated hydraulic conductivity K_s by Eq. (26) versus the measured values $K_{measured}$.

Fig. 8. The relationship between the fitted parameter n and the mass fraction of montmorillonite in bentonite-based materials ω.

Fig. 9. Predicted hydraulic conductivity K_s using Eq. (43) versus the measured values $K_{measured}$.

Fig. 10. Evolution of (a) SSA_{ca}/SSA_s and (b) ϕ_{ca}/ϕ with the mass fraction of montmorillonite and porosity.

Fig. 11. Comparison of Eq. (32) and the original VG model fitted to water retention data for the Kunigel-V1/sand mixture, GMZ bentonite, and MX-80 bentonite/Cox claystone mixture, with data from Cui et al. (2008), Ye et al. (2012), and Zeng et al. (2022), respectively.

Fig. 12. Comparison of measured and predicted hydraulic conductivities using Eq. (42) and the original VG-M equation for the Kunigel-V1/sand mixture, GMZ bentonite, and MX-80 bentonite/Cox claystone mixture, with data from Cui et al. (2008), Ye et al. (2012), and Zeng et al. (2022), respectively.

Fig. 13. Predicted relative hydraulic conductivity with S_{ad} determined by Eq. (31) (solid line) and as a fitted parameter (dashed line) for the Kunigel-V1/sand mixture, GMZ bentonite, and MX-80 bentonite/Cox claystone mixture, based on experimental data from Cui et al. (2008), Ye et al. (2012), and Zeng et al. (2022), respectively.

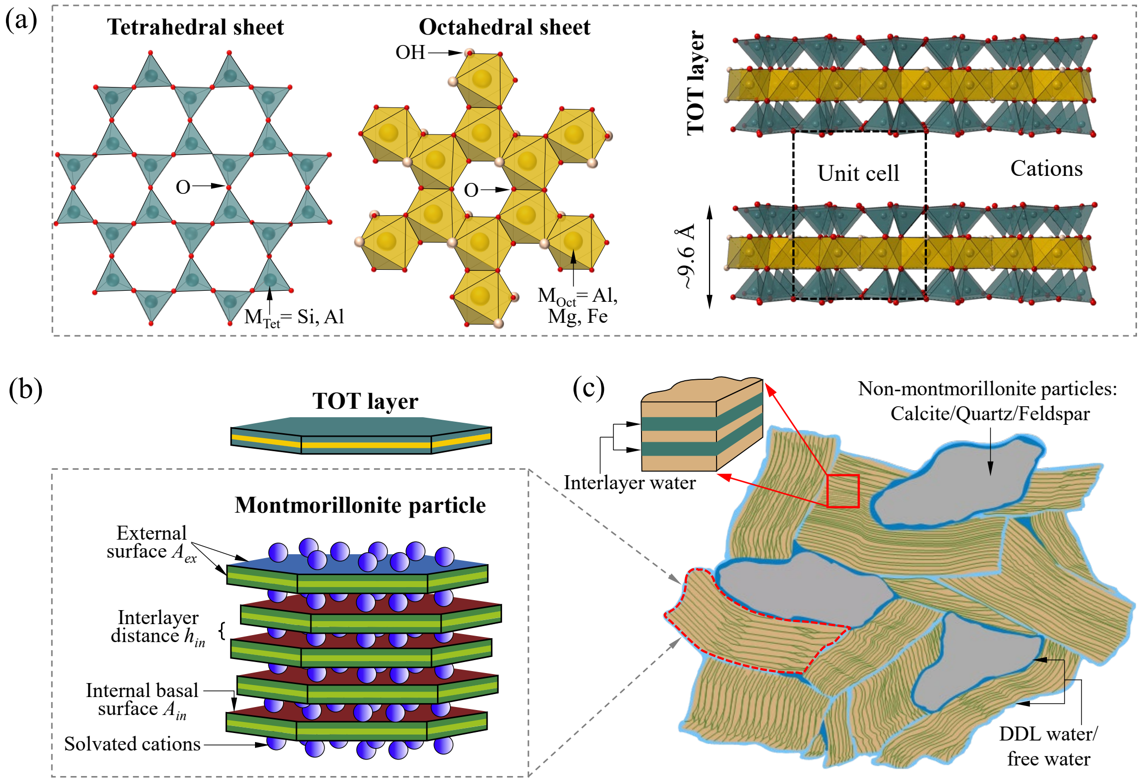

Fig. 1. Schematic diagram of microstructure and water types in bentonite-based materials (modified after Bradbury and Baeyens, 2003; Tournassat et al., 2015): (a) TOT layer and unit cell of montmorillonite, (b) formation of montmorillonite particle, and (c) water distribution.

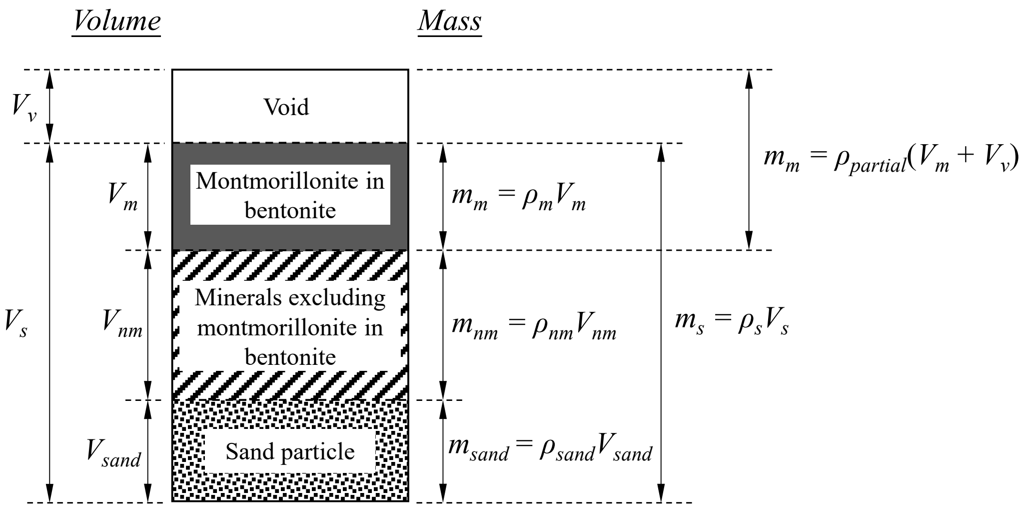

Fig. 2. Composition of bentonite-sand mixture and definition of the density of the soil particle ρ_s and partial dry density of montmorillonite $\rho_{m\text{-}partial}$.

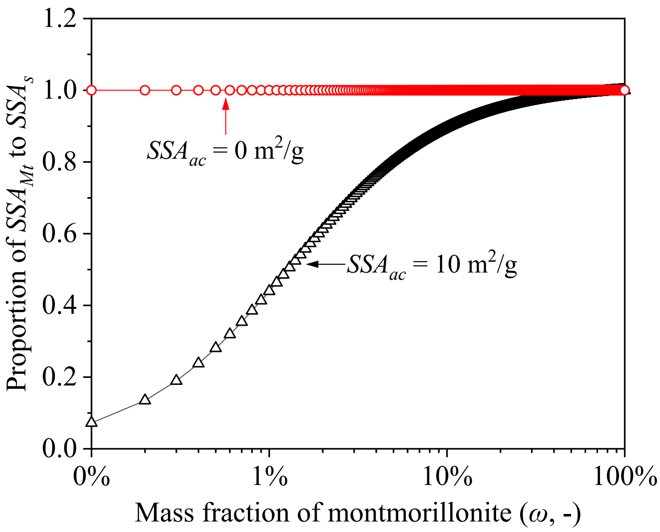

Fig. 3. Contributions of SSA_{Mt} to total SSA_s of bentonite. Subscript '*ac*' represents the non-montmorillonite minerals in bentonite-based materials.

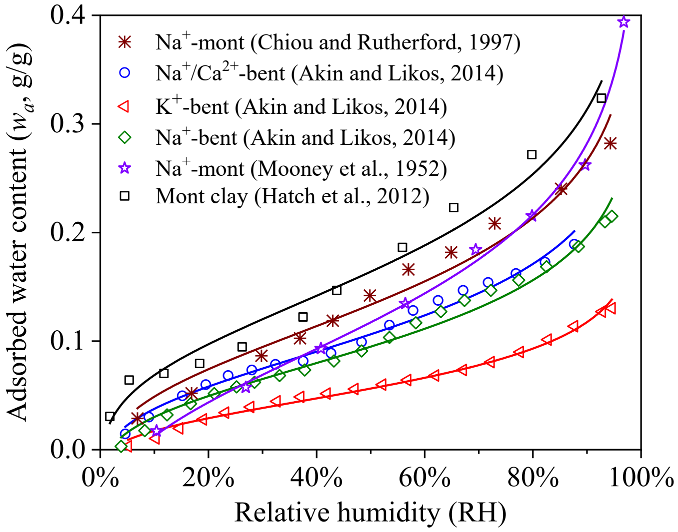

Fig. 4. Measured (data point) and predicted (solid line) soil water adsorption isotherms by Eq. (27) for bentonite materials.

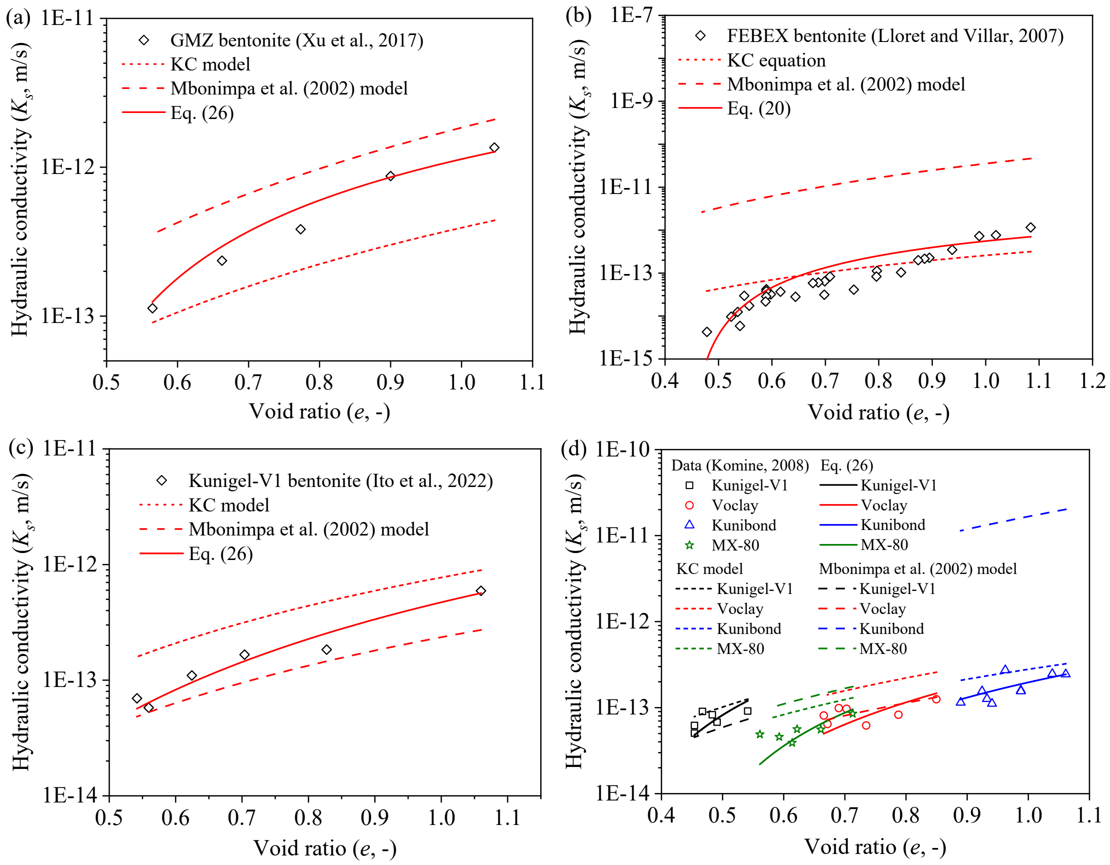

Fig. 5. Comparison of prediction saturated hydraulic conductivity for bentonite materials: conventional KC equation, Mbonimpa et al. (2002) model and the modified model of Eq. (26).

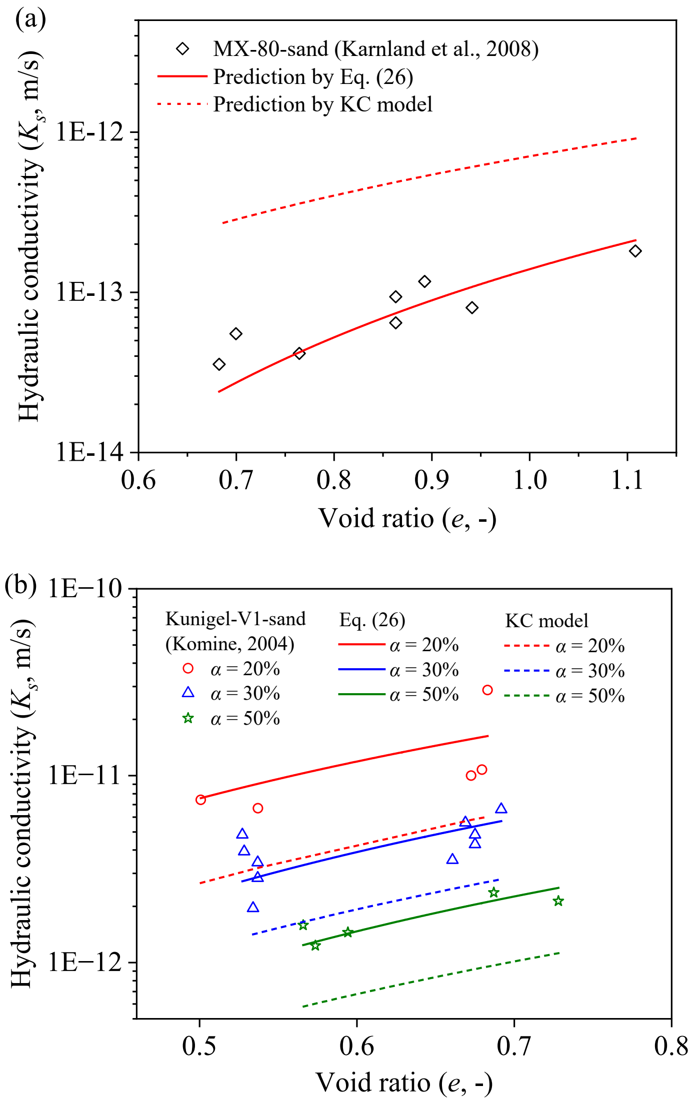

Fig. 6. Comparison of predicted saturated hydraulic conductivity for bentonite-sand mixtures: conventional KC equation and the modified model of Eq. (26).

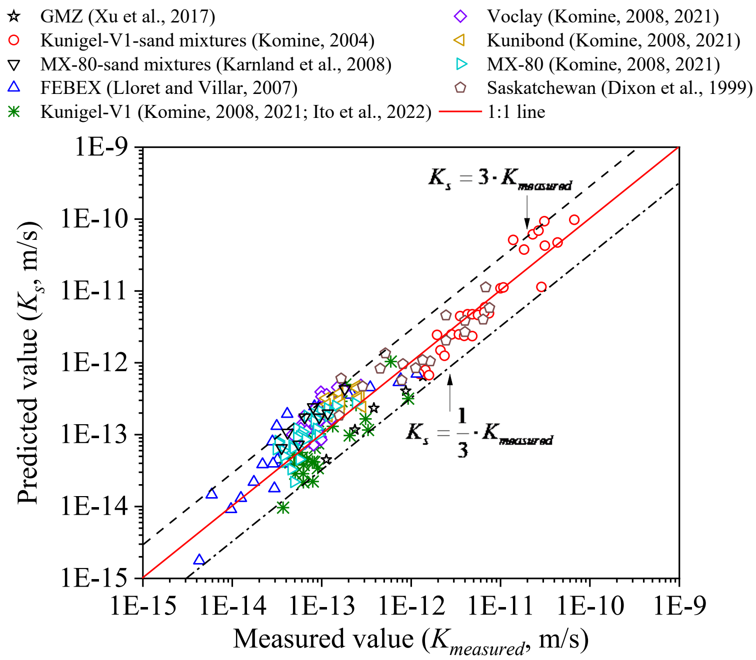

Fig. 7. The predicted saturated hydraulic conductivity K_s by Eq. (26) versus the measured values $K_{measured}$.

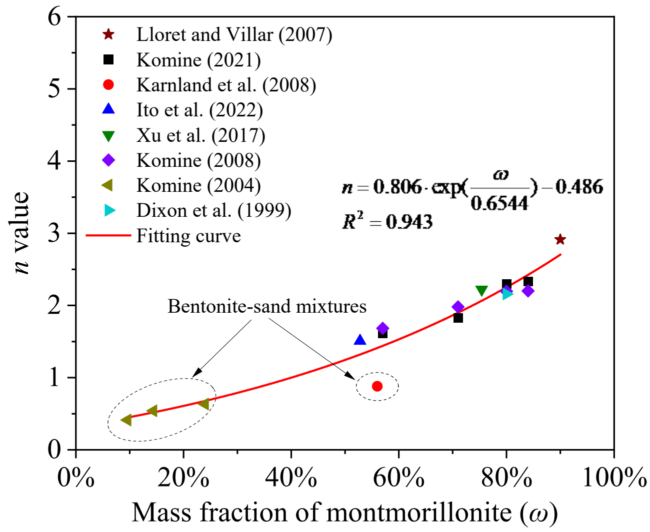

843

844 **Fig. 8.** The relationship between the fitted parameter n and the mass fraction of

845 montmorillonite in bentonite-based materials ω.

846

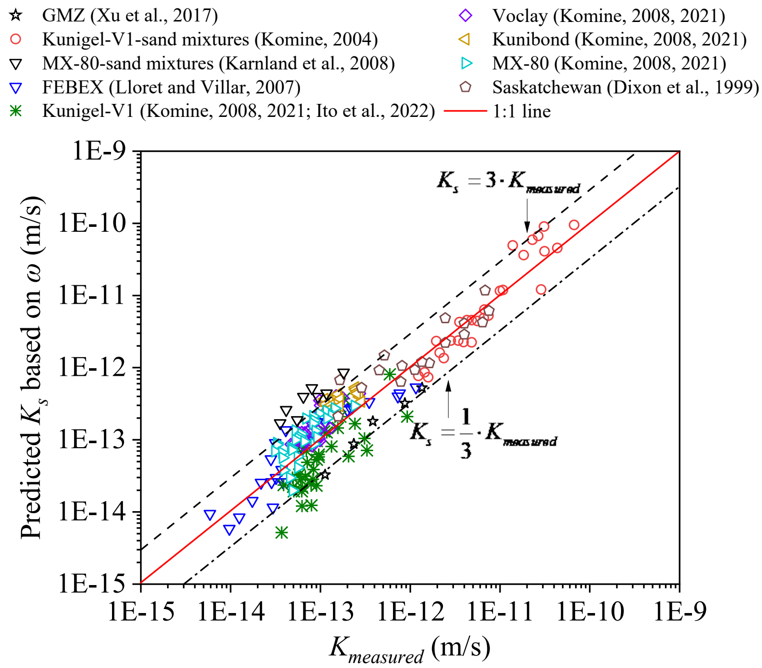

Fig. 9. Predicted hydraulic conductivity K_s using Eq. (43) versus the measured values $K_{measured}$.

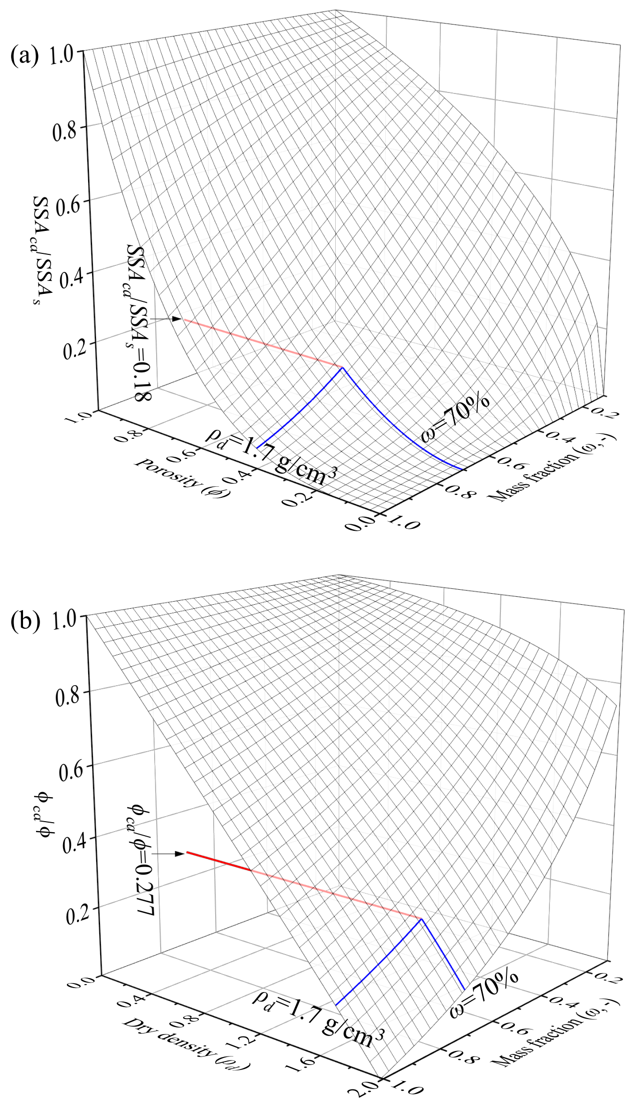

Fig. 10. Evolution of (a) SSA_{ca}/SSA_s and (b) ϕ_{ca}/ϕ with the mass fraction of montmorillonite and porosity.

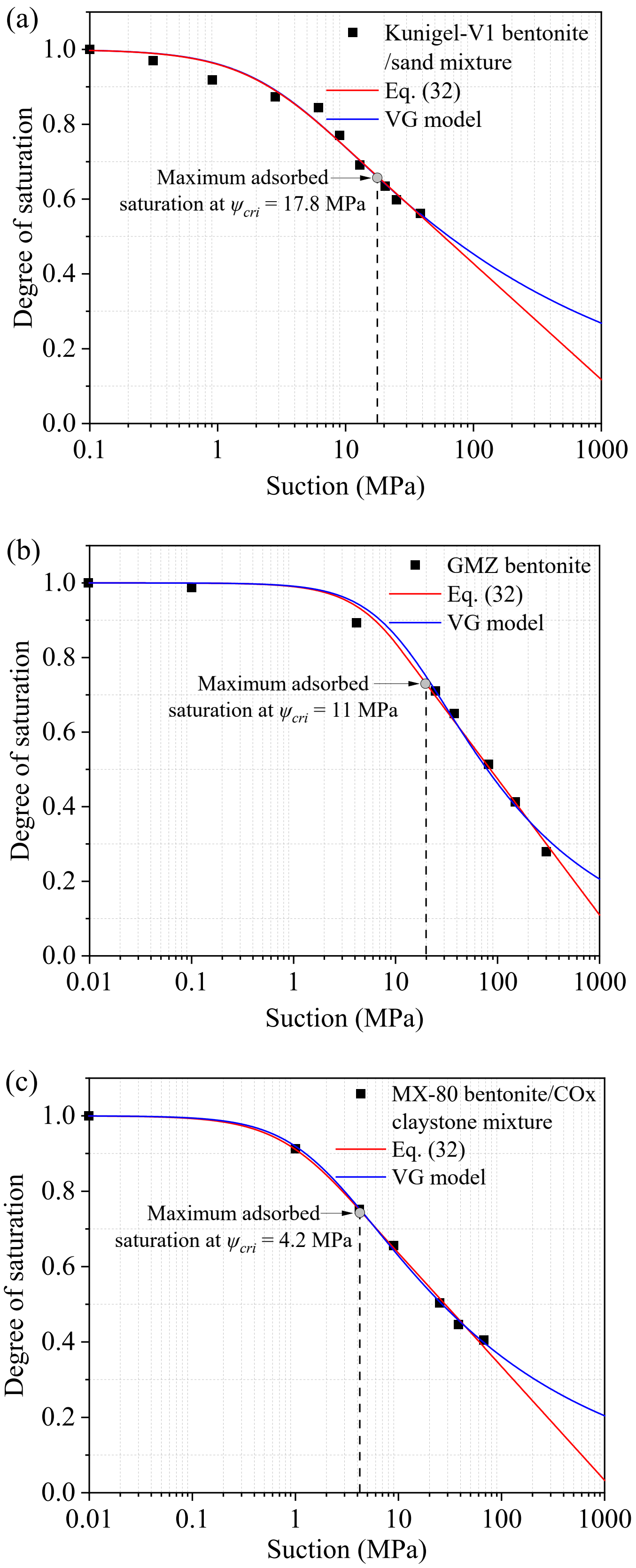

Fig. 11. Comparison of Eq. (32) and the original VG model fitted to water retention data for the Kunigel-V1/sand mixture, GMZ bentonite, and MX-80 bentonite/Cox claystone mixture, with data from Cui et al. (2008), Ye et al. (2012), and Zeng et al. (2022), respectively.

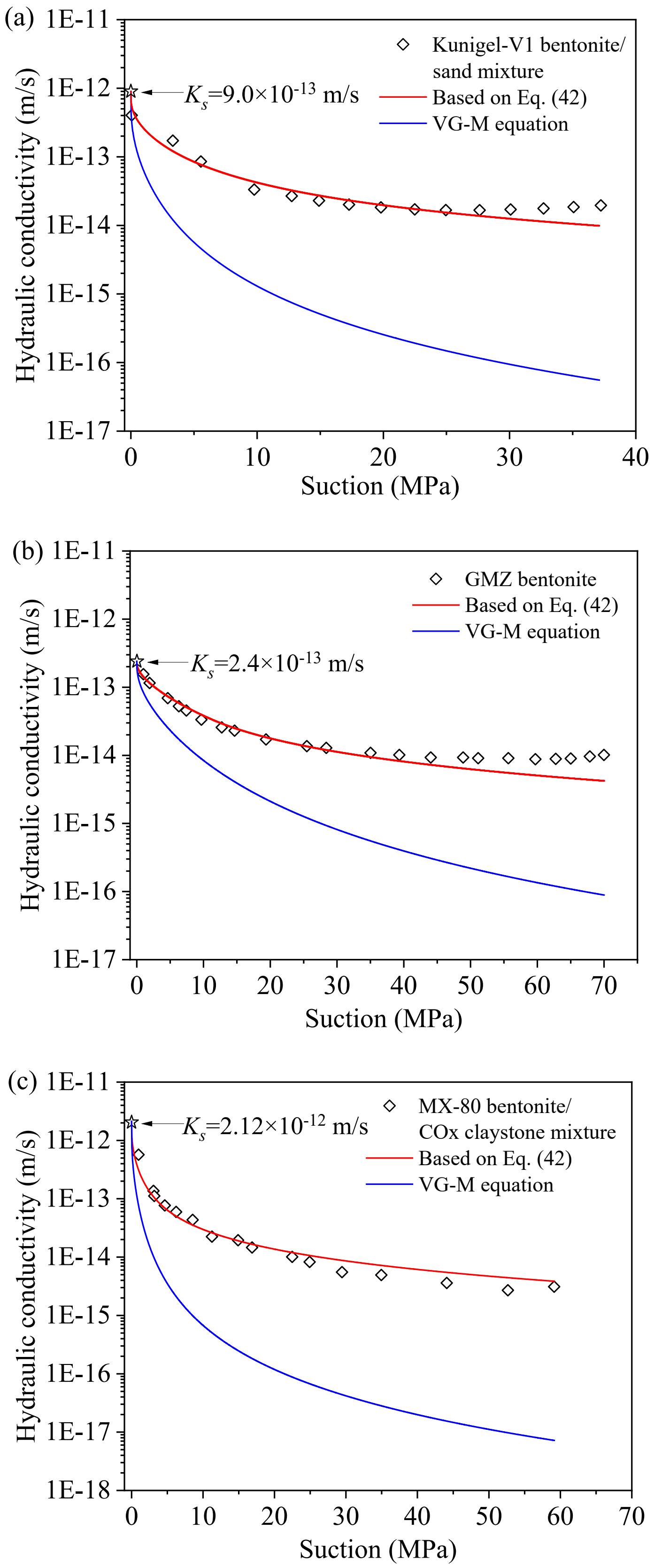

Fig. 12. Comparison of measured and predicted hydraulic conductivities using Eq. (42) and the original VG-M equation for the Kunigel-V1/sand mixture, GMZ bentonite, and MX-80

bentonite/Cox claystone mixture, with data from Cui et al. (2008), Ye et al. (2012), and Zeng et al. (2022), respectively.

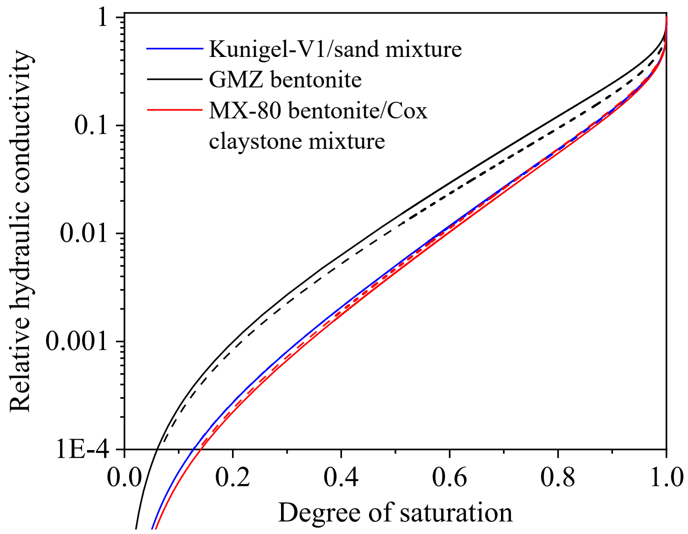

Fig. 13. Predicted relative hydraulic conductivity with S_{ad} determined by Eq. (31) (solid line) and as a fitted parameter (dashed line) for the Kunigel-V1/sand mixture, GMZ bentonite, and MX-80 bentonite/Cox claystone mixture, based on experimental data from Cui et al. (2008), Ye et al. (2012), and Zeng et al. (2022), respectively.

Table 1. Database for verification of the modified KC model on compacted bentonite.

Type of bentonite	Mass fraction of montmorillonite	Number of data points	Particle density (kg/m^3) [a]	Specific surface area [b] (m^2/g)	Testing method	Reference
FEBEX	90%	29	2700	725	Constant head gradients test	Lloret and Villar, 2007
GMZ	75.40%	5	2660	597	Constant head gradient test	Xu et al., 2017
Saskatchewan bentonite	80%	17	2840	519-613	Constant head gradient test	Dixon et al., 1999
Kunigel-V1	52.80%	6	2760	(410)	Falling head permeability test	Ito et al., 2022
Kunigel-V1	57%	24	2790	(442)	Consolidation test	Komine, 2021
Volclay	71%	22	2840	(551)	Consolidation test	Komine, 2021
Kunibond	84%	8	2710	(652)	Consolidation test	Komine, 2021
MX-80	80%	25	2880	(621)	Consolidation test	Komine, 2021
Kunigel-V1	57%	6	(2790)	(442)	Consolidation test	Komine, 2008
Volclay	71%	7	(2840)	(551)	Consolidation test	Komine, 2008
Kunibond	84%	9	(2710)	(652)	Consolidation test	Komine, 2008
MX-80	80%	6	(2880)	(621)	Consolidation test	Komine, 2008

[a] Particle density values in brackets were not sourced directly from the literature but were instead computed based on Eq. (13).
[b] The specific surface area values in brackets were determined according to $SSA_s = SSA_{Mt} \cdot \omega_1$.

Table 2. Database for verification of the modified KC model on bentonite-sand mixtures.

Type of bentonite	Mass fraction of montmorillonite ω_1	Type of sand	Bentonite content by mass α	Number of data points	Particle density (kg/m^3)	Testing method	Reference
MX-80	80%	Quartz sand	70%	8	(2740)	Constant head gradient test	Karnland et al., 2008
Kunigel-V1	48%	Mikawa	50%	5	(2726)	Consolidation test	Komine, 2004

silicate sand	30%	10	(2698)	Consolidation test
	20%	5	(2686)	Consolidation test

Table 3. Specifications for bentonite-based materials used for water retention and hydraulic conductivity tests.

Bentonite type	Mass fraction of montmorillonite	Partial dry density of montmorillonite [b] (kg/m^3)	Particle density (kg/m^3)	Dry density (kg/m^3)	Reference
Kunigel-V1/sand mixture	33.6%	1363	2670	2000	Cui et al., 2008
GMZ bentonite	75.4%	1521	2660	1700	Ye et al., 2012
MX-80 bentonite/Cox claystone mixture	53.8%[a]	1398	(2718)	1800	Zeng et al., 2022

[a] Mean value based on mass content of montmorillonite in both MX-80 bentonite and Cox claystone.
[b] Calculated by Eq. (18).

Table 4. Summary of parameters for the proposed SWRC model (Eq. (32)) and original VG model.

Bentonite type	Proposed model				Original VG model	
	Fitted parameters		Calculated parameters			
	ψ_{cri}	m	B	ψ_a	m	ψ_a
Kunigel-V1 bentonite/sand mixture	17.81	1.23	134.49	3.17	1.23	3.24
GMZ bentonite	11	1.38	181.99	10.87	1.36	11.97
MX-80 bentonite/Cox claystone mixture	4.2	1.22	305.86	1.36	1.25	1.67

Table 5. Summary of fitting results for Eq. (32) with S_{ad} set as a fitted parameter.

Bentonite type	Fitted parameters			Calculated parameters	
	S_{ad}	ψ_{cri}	m	B	ψ_a
Kunigel-V1 bentonite/sand mixture	0.71	12.01	1.23	194.3	3.12
GMZ bentonite	0.68	27.77	1.29	66.62	8.8
MX-80 bentonite/Cox claystone mixture	0.79	2.92	1.23	449.45	1.47